CellPress

Structure
Article

The LxVP and PxIxIT NFAT Motifs Bind Jointly to Overlapping Epitopes on Calcineurin's Catalytic Domain Distant to the Regulatory Domain

Maayan Gal,[1,2,3] Shuai Li,[1,2] Rafael E. Luna,[1] Koh Takeuchi,[1,4] and Gerhard Wagner[1,*]
[1]Department of Biological Chemistry and Molecular Pharmacology, Harvard Medical School, 240 Longwood Avenue, Boston, MA 02115, USA
[2]Co-first author
[3]Present address: Migal Research Center, Tarshish 1, Kiryat, Shmona, 11016, Israel
[4]Present address: Molecular Profiling Research Center for Drug Discovery, National Institute of Advanced Industrial Science and Technology, 2-3-26 Aomi, Koto, Tokyo 135-0064, Japan
*Correspondence: gerhard_wagner@hms.harvard.edu
http://dx.doi.org/10.1016/j.str.2014.05.006

SUMMARY

The serine/threonine phosphatase calcineurin (Cn) targets the nuclear factors of activated T cells (NFATs) that activate cytokine genes. Calcium influx activates Cn to dephosphorylate multiple serine residues within the ~200 residue NFAT regulatory domain, which triggers joint nuclear translocation of NFAT and Cn. The dephosphorylation process relies on the interaction between Cn and the conserved motifs PxIxIT and LxVP, which are located N- and C-terminal to the phosphorylation sites in NFAT's regulatory domain. Here, we show that an NFATc1-derived 15-residue peptide segment containing the conserved LxVP motif binds to an epitope on Cn's catalytic domain (CnA), which overlaps with the previously established PxIxIT binding site on CnA and is distant to the regulatory domain (CnB). Both NFAT motifs partially compete for binding but do not fully displace each other on the CnA epitope, revealing that both segments bind simultaneously to the same epitope on the catalytic domain.

INTRODUCTION

The nuclear factors of activated T cells (NFATs) are transcription factors that regulate numerous genes upon T cell activation (Hogan et al., 2003; Rao et al., 1997; Serfling et al., 2000). They upregulate cytokines required for T cell proliferation and stimulate cell growth and differentiation during the T cell response (Kiani et al., 2000). Four of the five known NFAT proteins are part of the T cell response mechanism (Macian, 2005), but NFAT proteins also take part in different regulatory mechanisms of other cells (Crabtree and Olson, 2002; Graef et al., 2001; Hogan et al., 2003; Kao et al., 2009). The C-terminal half of the 930-residue NFAT contains two domains involved in binding DNA and AP-1 and has been characterized structurally (Chen et al., 1998; Jin et al., 2003; Wolfe et al., 1997; Zhou et al., 1998). The N-terminal half known as the NFAT homology region (NHR) contains a transactivation domain (TAD) and a regulatory domain (Figure 1A). The regulatory domain of approximately 200 residues contains a nuclear localization region (NLS), 3 serine-proline (SP)-rich repeats, and 2 serine-rich regions (SRR). Phosphorylation status of these segments controls NFAT nuclear import and export by yet unknown mechanisms. In resting T cells, the regulatory domain is heavily phosphorylated, preventing NFAT from entering the nucleus. Four kinases are known to phosphorylate NFAT: casein kinase 1 (CK1), glycogen synthase kinase 3 (GSK3), protein kinase A (PKA), and the dual specificity tyrosine phosphorylation kinase (DYRK) (Arron et al., 2006; Gwack et al., 2006; Okamura et al., 2000; Okamura et al., 2004). Rising Ca^{2+} levels, such as caused by mitogens, activate the calcium-dependent phosphatase calcineurin (Cn), a heterodimeric protein consisting of a catalytic domain (CnA) and a calmodulin-like regulatory domain (CnB). CnB constitutively binds to the C-terminal side of CnA to form the heterodimer (hereafter we call the heterodimeric CnA/CnB complex CnAB). Following activation, Cn dephosphorylates NFAT and initiates joint nuclear translocation of both NFAT and Cn (Shibasaki et al., 1996). The nuclear entry event also involves other proteins, such as importin-β and tubulin-α (Ishiguro et al., 2011). In the nucleus, NFAT assembles with other transcription factors and coactivators to initiate the immune response (Flanagan et al., 1991; Jain et al., 1992; Wu et al., 2007).

Two distinct Cn-binding segments have been identified in the NHR of all NFAT isoforms involved in T cell response. They contain the conserved PxIxIT and LxVP motifs and are labeled CN-1 and CN-2 in Figure 1A. The NHR was found unstructured, both in its active and inactive states (Park et al., 2000). The PxIxIT motif was discovered first and is highly conserved among NFAT isoforms (Aramburu et al., 1998; Zhu et al., 1998). Peptides containing the endogenous PxIxIT sequence (PRIEIT in NFATc1/c2) bind calcineurin with low to midmicromolar affinities (Aramburu et al., 1998). The nonconserved amino acids (x) in positions 2 and 4 modulate the binding affinities, and these residues are thought to cause fine-tuning of this interaction under different physiological conditions (Li et al., 2007). Affinity-driven selection of peptide inhibitors resulted in an optimized peptide that binds Cn with a 200 nM dissociation constant (K_D). Residues in

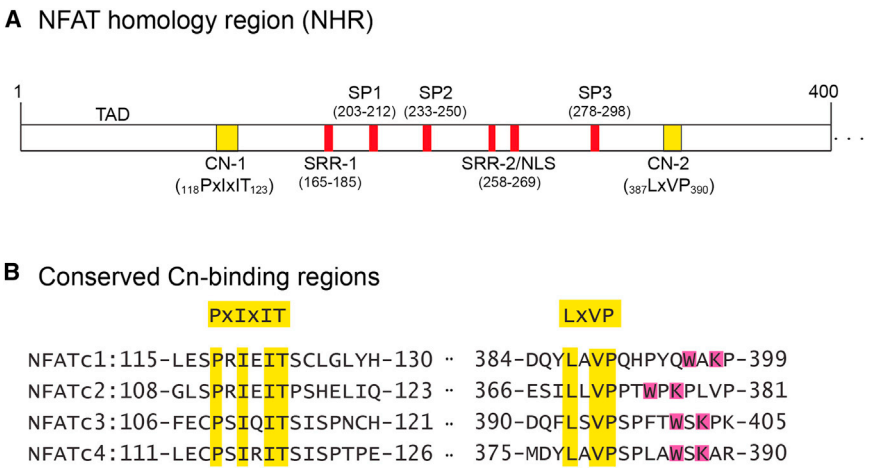

Figure 1. Location of Functional Segments in NFAT's Homology Region

(A) Sequences of Cn-binding regions. Residues conserved throughout the different human NFAT isoforms are highlighted in yellow. The following abbreviations are used to represent the functional segments: TAD, transactivation domain; CN-1 and CN-2, the conserved binding motifs of Cn PxIxIT and LxVP; SRR-1 and SRR-2, serine-rich regions; SP1, SP2, and SP3, serine-proline rich repetition segments; NLS, nuclear localization sequence.

(B) NFAT-conserved motifs, PxIxIT and LxVP, primary amino acid sequences throughout the different human NFAT isoforms.

positions x were selected as valines yielding the PVIVIT sequence (Aramburu et al., 1999; Li et al., 2011). Structures of CnAB and CnA in complex with a 14-mer NFAT peptide containing the PVIVIT sequence have been determined with X-ray crystallography (Li et al., 2007) and nuclear magnetic resonance (NMR) spectroscopy (Takeuchi et al., 2007).

More recently, a second Cn-binding segment was discovered that contains the conserved LxVP sequence. Located C-terminal to NFAT's regulatory domain, it binds Cn with similar affinity as the PxIxIT segment. Furthermore, it was observed that blocking the interaction of Cn with the PxIxIT motif alone does not prevent NFAT nuclear translocation. Thus, it was concluded that the interaction of Cn with the LxVP motif is necessary for an efficient dephosphorylation process (Liu et al., 1999; Park et al., 2000).

Because of its role in T cell activation, Cn has been targeted for development of immune-suppressive drugs. The most successful Cn inhibitors discovered so far, cyclosporin A (CsA) and tacrolimus (FK506), block Cn's phosphatase activity by obscuring its catalytic site. They are presented as stable dimeric complexes with the intracellular proteins cyclophilin or FKBP12, respectively (Griffith et al., 1995; Huai et al., 2002; Kissinger et al., 1995). More recently, significant effort has been made to specifically inhibit the Cn-NFAT complex formation without blocking Cn's catalytic activity, thus leading to a more selective agent by enabling Cn to continue with its other roles (Roehrl et al., 2004a, 2004c). For that purpose, the inhibition of the PxIxIT site was extensively pursued, whereas less effort was directed toward blocking the LxVP interaction due to lack of structural data (Lee and Park, 2006; Zhou et al., 2011).

Recently, it was suggested based on mutations and docking calculations that a peptide containing the NFAT-LxVP motif binds a region near the interface of CnA and CnB (Rodríguez et al., 2009). An LxVP binding site was also suggested based on a cocrystal structure of CnAB with the viral inhibitor protein A238L, which binds the CnA/B interface with an FLCVK motif (Grigoriu et al., 2013). Besides the P/K replacement, the LxVK segment also lacks the flanking residues found in NFAT's LxVP segments, some of which were recently shown to be important for its activity (Rodríguez et al., 2009).

Here, we present evidence that a 15-mer peptide from NFATc1 containing the conserved LxVP sequence binds to a CnA region overlapping with the PxIxIT-binding epitope. NMR competition experiments show that the LxVP and PxIxIT peptides partially displace each other at equimolar concentrations, suggesting that they bind simultaneously at overlapping binding epitopes, where they interact with each other. This contradicts previous proposals that the two motifs bind at two distant Cn sites. Our conclusion is supported by biophysical and atomic resolution data obtained through NMR spectroscopy and fluorescence polarization (FP) measurements. Our findings suggest that it should be possible to inhibit the Cn/NFAT interaction with a single inhibitory molecule, which would have been difficult with two distant binding sites.

RESULTS

To characterize calcineurin binding of NFAT's homology domain, we selected two NFAT peptides containing the PxIxIT or LxVP motifs, respectively (Figure 1). The locations of the motifs in the NFAT homology region (NHR) are depicted in Figure 1A and are labeled CN-1 and CN-2, respectively. Figure 1B shows sequence alignments for both segments of the four T-cell-related human NFAT isoforms. Note that there is a WxK motif C-terminal to the LxVP sequence, which motivated us to use the longer 15-residue segment of NFATc1 for our binding studies. Indeed, the WxK motif seems to be important for activity of the LxVP motif (see below), which is consistent with previous studies (Rodríguez et al., 2009).

The CnA construct used here is identical to that described in previous structural and functional studies (Kang et al., 2005; Roehrl et al., 2004c). It comprises residues 2–347 of the native human CnA with Y341S, L343A, and M347D substitutions that increase protein solubility for NMR experiments. These mutated residues are located >20 Å away from the active site and do not affect the enzymatic activity of CnA. The heterodimeric CnAB used here contains the native sequence.

The NFATc1-Derived LxVP Peptide Interacts with CnA

To determine whether the NFAT-LxVP peptide binds CnA alone or requires the entire CnAB heterodimer, we compared NMR spectra of the ^{15}N-labeled peptide alone and upon addition of either CnA or CnAB. Figure 2A shows a heteronuclear single-quantum coherence (HSQC) spectrum of unbound ^{15}N-labeled NFAT-LxVP peptide, and Figure 2B is an expansion

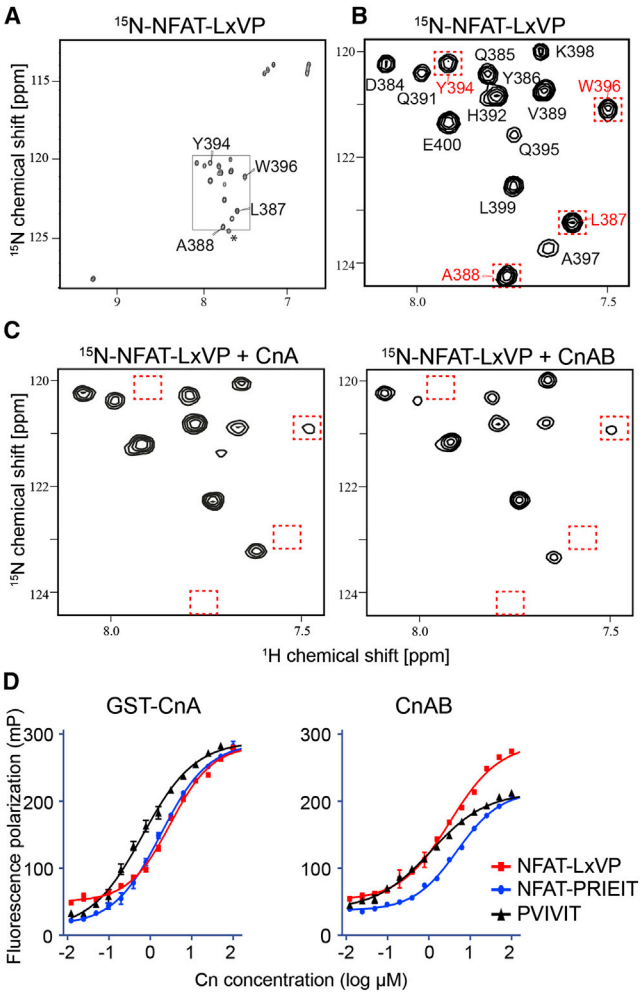

Figure 2. The NFAT-LxVP Peptide Interacts with CnA of Cn

(A) 2D ^{1}H-^{15}N HSQC spectrum of free 62 μM ^{15}N-labeled NFAT-LxVP peptide. The signal marked with an asterisk is an extra residue of the C-terminal His tag and is not relevant in this context.

(B) Inset of Figure 2A, which contains the relevant peaks and serves as a reference for the panels below.

(C) 2D ^{1}H-^{15}N HSQC spectra of ^{15}N-NFAT-LxVP peptide in the presence of nonlabeled CnA (left) and nonlabeled CnAB (right), which was acquired at an LxVP:Cn molar ratio of 1:1.2. In all 2D spectra, ten contour plot levels are drawn starting at 1.5 × 10^{5} and increasing by a factor of 1.40 for each additional level. Peak heights for complexes of ^{15}N-NFAT-LxVP peptides with CnA and CnAB are documented in the bar graphs of Figures 4 and S2.

(D) Semilogarithmic plots of fluorescence polarization experiments for determining K_D of NFAT-LAVP (red), NFAT-PRIEIT (blue), and PVIVIT (black) peptides. Each FITC-labeled peptide (30 nM) was incubated with increasing amounts of the GST-CnA (left) and CnAB (right). The binding affinity was determined using the software GraphPad Prism6 by fitting the data to a single-site binding model. Note that a dimeric GST fusion construct was used for CnA to increase the molecular mass of the complex and increase the fluorescence anisotropic difference between bound and free peptide. Thus, the bound FP of GST-CnA is larger than that of CnAB.

with all signals, except the C-terminal histidine. Next, we added either nonlabeled CnA (Figure 2C, left) or nonlabeled CnAB (Figure 2C, right) to ^{15}N-labeled NFAT-LxVP. Very similar spectral changes are observed: the same peaks are broadened, leading to reduced peak heights when adding either the CnA or the CnAB. Most affected are L387 and A388 of the LAVP motif and Y394 and W396 of the C-terminal flanking sequence (Figure 1). Broadening of peptide peaks upon binding to larger proteins is typically seen for residues contacting the larger molecule due to immobilization and slower tumbling and/or exchange between slightly different bound conformations.

Table 1. Equilibrium Dissociation Constants for the NFAT-LxVP and PxIxIT Peptide Interactions with CnA and CnAB

	CnA	CnAB
LxVP	K_D = 3.1 ± 0.44 μM	K_D = 3.2 ± 0.70 μM
PRIEIT	K_D = 2.5 ± 0.76 μM	K_D = 4.2 ± 1.1 μM
PVIVIT	K_D = 0.53 ± 0.11 μM	K_D = 0.51 ± 0.13 μM

The equilibrium dissociation constants were measured using the fluorescence polarization assay from Figure 2D.

Figure 2C shows that the same set of signals of the LxVP peptide are broadened upon binding to either CnA or CnAB. This indicates a similar binding mode to both CnA and CnAB and suggests LxVP's binding to the common moiety CnA. Some residues exhibit slightly different broadening behavior when titrating CnA or CnAB. For example, the intensity reduction of the signal originating from Q391 is more pronounced when bound to CnAB. This may be the result of exchange between slightly different bound conformations in the presence of the heterodimer CnAB or the higher molecular weight of the CnAB complex with NFAT-LxVP. It may also be due to a more anisotropic tumbling of the elongated CnAB compared to the more spherical CnA.

Next, we asked whether the presence of CnB causes tighter binding of the LxVP peptide. Using a FP assay (Roehrl et al., 2004b, 2004c), we measured affinities of fluorescein-tagged NFAT-LxVP peptide to CnA (glutathione S-transferase [GST]-tagged; GST-CnA) or CnAB. Figure 2D shows FP titrations of GST-CnA (left) and CnAB (right) to samples of NFAT-LxVP (red), NFAT-PRIEIT (blue), and the affinity-enhanced PVIVIT (black line) peptides. Fitting with a single-site binding model yields the K_D values in Table 1, which are consistent with the K_D of 2.5 μM measured previously with isothermal titration calorimetry (ITC) for the LxVP peptide (Park et al., 2000). The structure of the complex of the affinity-optimized PVIVIT peptide with calcineurin and the PVIVIT affinity to CnA are well established and serve as positive controls. Indeed, the obtained K_D suggests that our experimental conditions are congruent with previously reported data, indicating a dissociation constant of about 0.5 μM between the PVIVIT peptide and Cn (Roehrl et al., 2004a, 2004c). These results show that the NFAT-LxVP peptide binds to either CnA alone or CnAB with similar affinity, and the presence of CnB does not enhance binding of the LxVP peptide.

To verify these results with an orthogonal method, we measured direct binding of His-GB1-NFAT-PRIEIT and His-GB1-NFAT-LxVP to GST-CnA using BLItz technology, which yields association and dissociation rates and equilibrium dissociation constants. We found that the NFAT-PRIEIT peptide has 10-fold faster association and dissociation rates than does NFAT-LxVP. However, the K_D values measured with BLitz are almost identical for both peptides at 0.64 and 0.46 μM, respectively

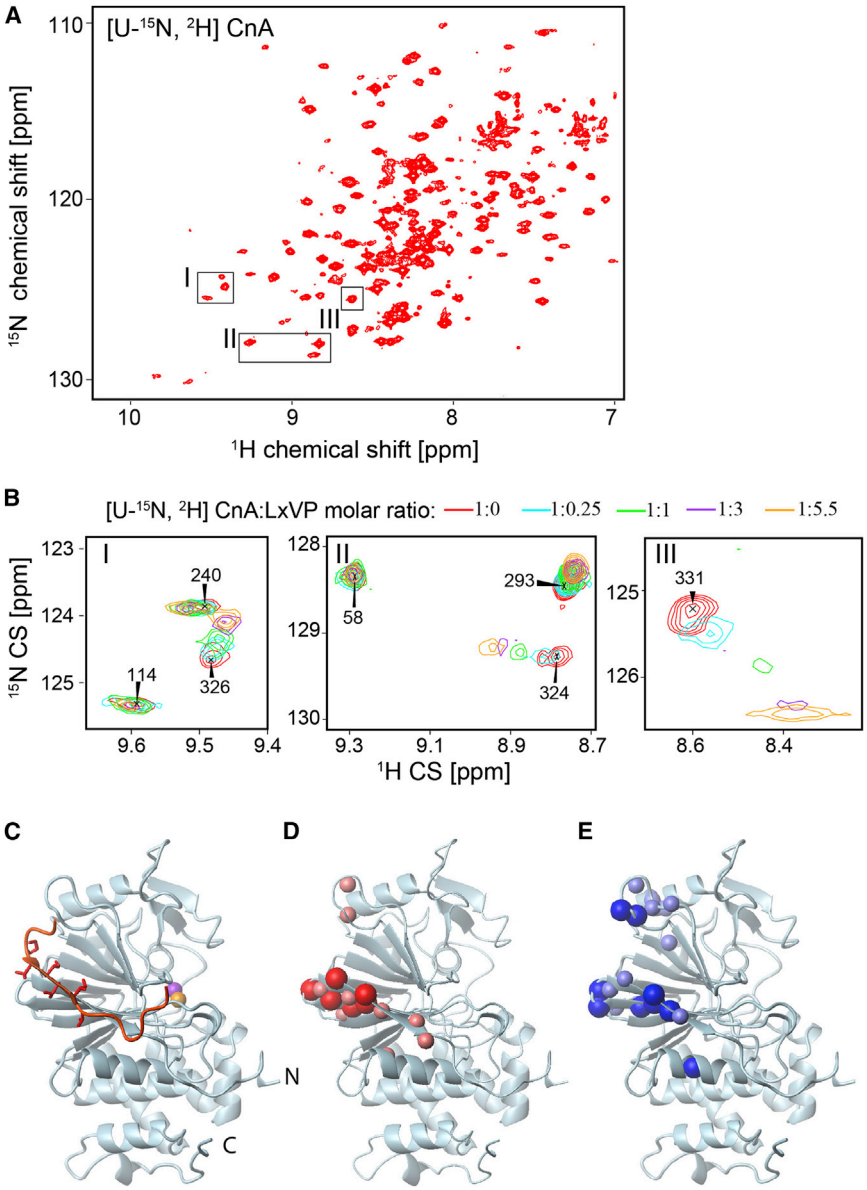

Figure 3. Characterization of the CnA: NFAT-LxVP Binding Epitope by NMR Spectroscopy

(A) 2D ^{1}H-^{15}N TROSY-HSQC NMR spectrum of [U-^{2}H^{15}N] CnA. The spectrum was acquired on a 600 MHz spectrometer with 2,048 (10 ppm) × 128 (30 ppm) complex points (SW) in the direct and indirect dimensions, respectively.

(B) Insets of representative regions from the series of the 2D HSQC TROSY-NMR spectra acquired during the titration of unlabeled NFAT-LxVP peptide (residues 384–400 of NFATc1) to [U-^{2}H^{15}N] CnA (residues 2–347). The spectra show CnA peaks in the absence of NFAT-LxVP (red) and in the presence of 1:0.25 (cyan), 1:1 (green), 1:3 (purple), and 1:5.5 (yellow) CnA:NFAT-LxVP molar ratios as depicted in the color legend on top of the panels. A complete record of the chemical shift perturbations for the assigned signals of CnA together with paramagnetic relaxation enhancement experiments are shown in Figure S1.

(C) Solution structure of the complex of CnA (gray) with a 15-residue PVIVIT peptide (Takeuchi et al., 2007). The active-site metals (Zn/Fe) are shown with solid spheres.

(D) Residues of CnA that exhibit chemical shift changes upon binding the PVIVIT peptide.

(E) Residues of CnA that exhibit chemical shift changes upon binding to the 15-residues NFAT-LxVP peptide. Large and small spheres represent chemical shift differences larger than 0.1 and 0.05 ppm, respectively.

(Figure S3 and Table S1 available online). This is consistent with previous reports (Liu et al., 1999; Park et al., 2000) and confirms that the NFAT- PRIEIT and NFAT-LxVP peptides bind CnA with equal affinities.

The NFAT-LxVP and PVIVIT Peptides Bind to Overlapping Epitopes on CnA

Having established that NFAT-LxVP binds to CnA, we turned to identify the exact binding epitope at a residue level using NMR-chemical shift perturbation (CSP). We titrated nonlabeled NFAT-LxVP peptide into an NMR sample of ^{15}N, ^{2}H-CnA. Figure 3A shows a 2D ^{1}H-^{15}N-correlated TROSY-HSQC spectrum of the 40 kDa CnA alone. We then titrated the nonlabeled NFAT-LxVP peptide (Figure 1B) and followed the CSP of CnA in 2D TROSY-HSQC spectra. Figure 3B shows three insets from different regions of the CnA HSQC spectra (boxed in Figure 3A), wherein both types of shifted and nonshifted residues can be observed. The shifted residues showed fast-to-intermediate exchange, which is typical for low micromolar interactions.

Because the bound structure of the PVIVIT peptide is known, we compared the CnA chemical shift changes upon binding of the PVIVIT (Figure S1A) and NFAT-LxVP peptides (Figure S1B). In addition to the chemical shift changes documented in Figures S1A and S1B, some residues experience severe line broadening during the addition of the NFAT-LxVP peptide as they appear to reach the limit of intermediate exchange. Residues with the largest changes are listed in the supplement (Figure S1). This pattern is similar, but not identical, to that of the PVIVIT peptide.

Note that we have incomplete assignments for the CnA construct used here. The residues around the paramagnetic center of the protein are not assigned due to paramagnetic line broadening. Moreover, because the protein was expressed in D_2O, we lack the assignments for residues located in the hydrophobic core that did not back exchange amides ^{2}H to ^{1}H. Yet, most surface residues away from the paramagnetic center are assigned, and the identification of the binding epitope is complete. Moreover, the assignments of the binding epitope have been validated by structure determination of the Cn/VIVIT peptide complex (Li et al., 2007; Takeuchi et al., 2007).

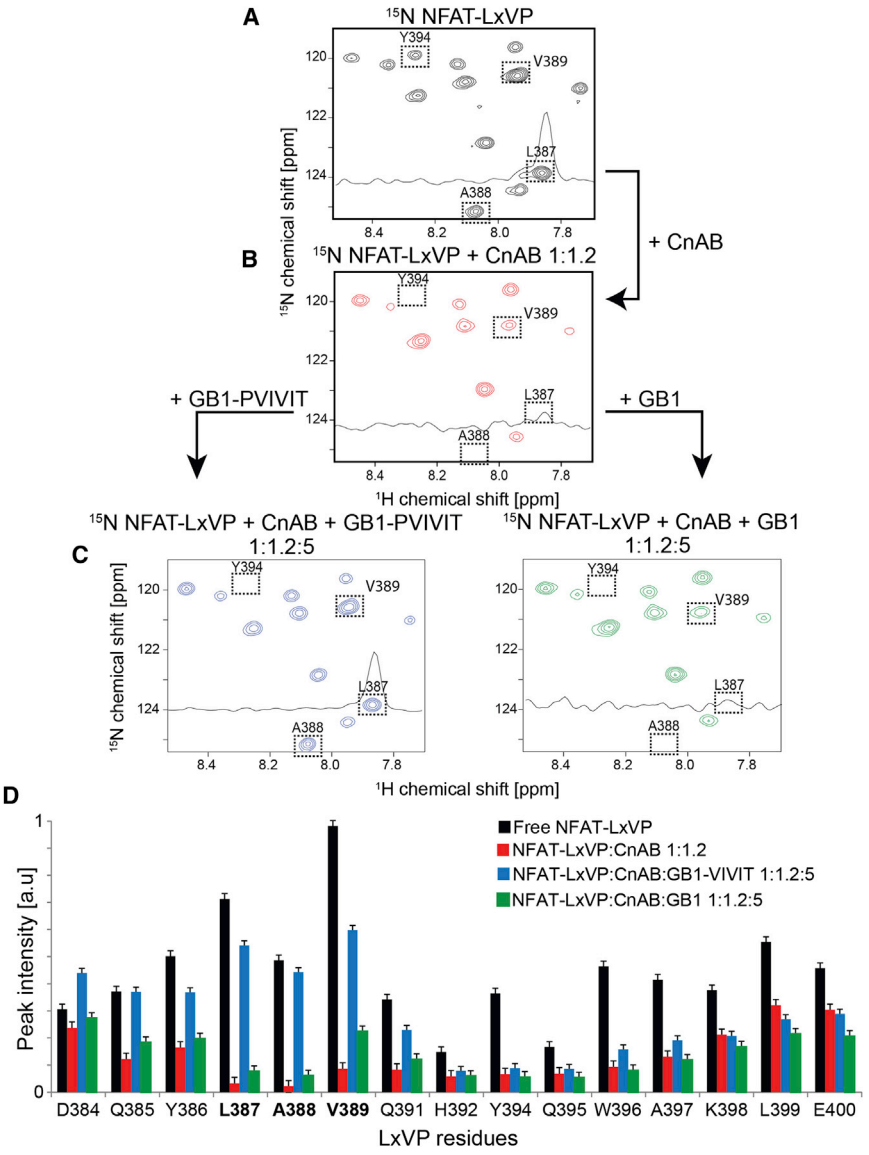

Figure 4. PVIVIT Competes out NFAT-LxVP from CnAB

(A–C) 2D ^{1}H-^{15}N HSQC spectra of the following: (A) 62 μM ^{15}N-labeled NFAT-LxVP alone. (B) ^{15}N-labeled NFAT-LxVP in a complex with CnAB in 1:1.2 molar ratio. Peaks of the residues contacting CnAB are strongly reduced, and some are also slightly shifted. (C) Addition of unlabeled His_6-GB1-PVIVIT (left) in a 1:1.2:5 molar ratio restores intensity of some peaks (L387, A388, and V389; the LxV of LxVP motif), but not of others (Y294, W396, A397, and K398; the WxK motif). Addition of unlabeled His_6-GB1 as a control (right) does not restore the intensity changes. The spectra were acquired on a 600 MHz spectrometer with 2,048 (10 ppm) × 128 (30 ppm) complex points (spectrum width [SW]) in the direct and indirect dimensions, respectively. In order to document the intensity changes, cross-sections are drawn through the peak of L387 in all four panels.

(D) Bar graph indicating the relative peak intensity of NFAT-LxVP peaks corresponding to each of the four spectra in (A)–(C) with peak colors similar to the representative bars. The error bars indicate the noise levels in the respective spectra as extracted from SPARKY using median of 10,000 calculated points.

The CnA signal changes upon peptide binding indicate both direct and indirect interactions, such as allosteric effects. To detect only direct spatial-related interaction, we used paramagnetic relaxation enhancement (PRE). We attached the methanethiosulfonate (MTSL) spin label to the thiol of mutated Q385C in the second position of the LxVP peptide. We compared the intensities of CnA backbone NH cross-peaks when bound to NFAT-LxVP-MTSL before and after reducing the spin label with ascorbic acid (Figure S1C). Residues most affected coincide with the known PVIVIT binding region on CnA, confirming that both peptides bind to a common epitope.

To visualize the NMR mapping of the peptide binding, Figure 3C shows a cartoon of CnA in complex with the PVIVIT peptide (orange colored) (Takeuchi et al., 2007). The CnA residues with the largest chemical shift changes upon binding the PVIVIT and NFAT-LxVP peptides are indicated with red and blue spheres in Figures 3D and 3E, respectively. As can be seen, the similarity of the sets of Cn residues that interact with PVIVIT or NFAT-LxVP reveals that the two peptides bind approximately the same epitope on CnA. However, the NFAT-LxVP peptide affects more strongly a helical region above the PVIVIT binding site (top left of Figure 3E). Thus, the residues that are perturbed upon binding by both peptides on CnA are overlapped but are not identical.

The PxIxIT and LxVP Motifs Compete for Binding to CnAB, but Only Partially

Having shown that both NFAT-LxVP and PVIVIT-containing peptides bind to an overlapping surface of CnA, we asked whether the two motifs bind competitively. First, we recorded ^{1}H-^{15}N-correlated spectra of ^{15}N-labeled NFAT-LxVP alone (Figure 4A) and following the addition of unlabeled CnAB (Figure 4B) similar to Figure 2C. In a second step, we added the unlabeled PVIVIT peptide to the complex to see whether it competes out the ^{15}N-labeled NFAT-LxVP peptide. Four peaks that display strongest intensity changes (L387, A388, V389, and Y394) are labeled in the spectra. In order to document the size of the intensity losses, cross-sections are drawn for L387 as a representative case. Addition of unlabeled GB1-PVIVIT to this sample (Figure 4C, left panel) leads to the reappearance of some of the affected signals (L387, A388, and V389; the residues of the LxVP segment), whereas others remain suppressed (Y394). As a negative control, addition of GB1 alone does not produce this effect (Figure 4C, right panel). In addition, we verified that the GB1 protein did not interact with the NFAT-LxVP segment by recording 2D HSQC spectra of ^{15}N-labeled GB1 with and without the NFAT-LxVP peptide (Figure S4). A complete

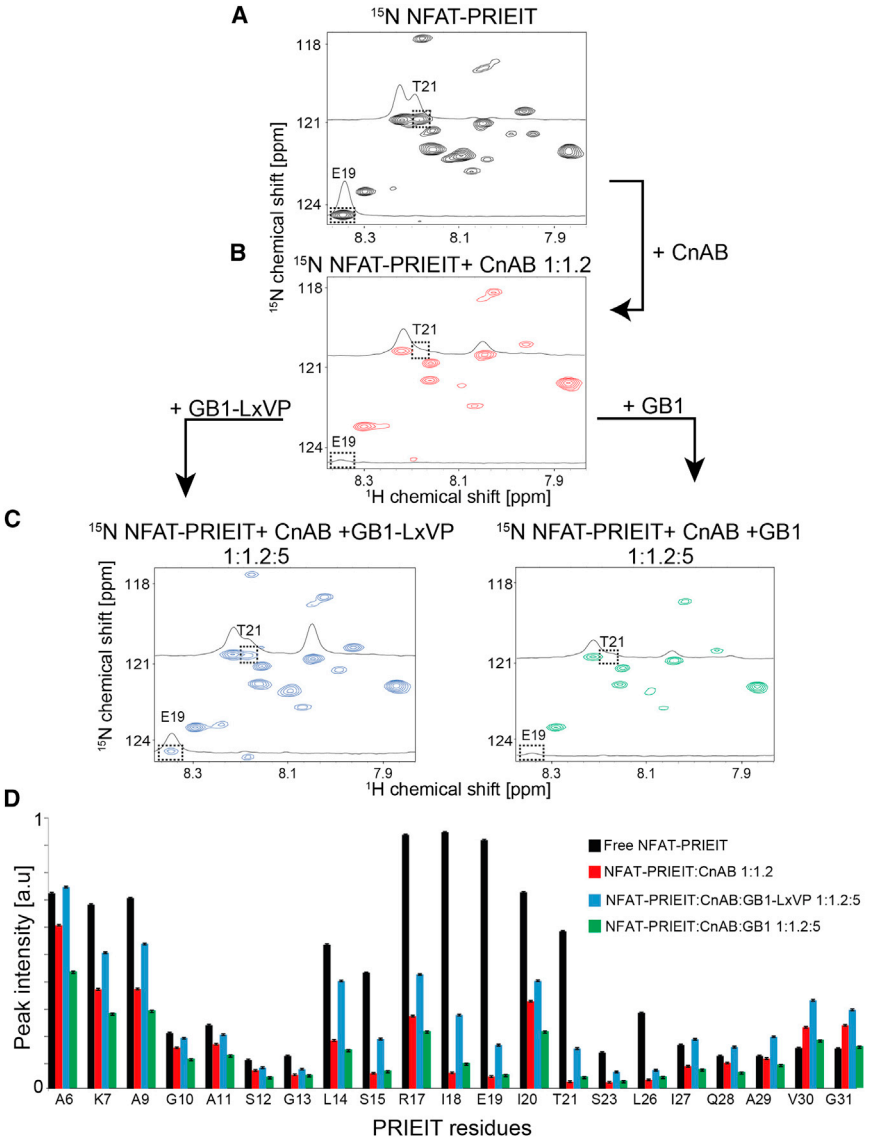

Figure 5. GB1-LxVP Partially Displaces ^{15}N-PxIxIT from CnAB

(A–C) 2D ^{1}H-^{15}N HSQC spectra of the following: (A) 75 μM ^{15}N-labeled NFAT-PRIEIT alone, (B) ^{15}N-labeled NFAT-PRIEIT in a complex with heterodimer CnAB in 1:1.2 molar ratio, (C) and addition of GB1-LxVP-His$_6$ (C-left) and unlabeled His$_6$-GB1 (C-right) in a 1:1.2:5 molar ratio. The spectra were acquired on a 600 MHz spectrometer with 2,048 (10 ppm) × 128 (30 ppm) complex points (SW) in the direct and indirect dimensions, respectively. In order to document the intensity changes, cross-sections are drawn through the peaks of T21 and E19 in all four panels.

(D) Bar graph reporting the intensities of NFAT-PRIEIT peaks corresponding to each of the different spectra from (A)–(C) with peak colors similar to the representative bars. The error bars indicate the noise levels in the respective spectra as extracted from SPARKY using median of 10,000 calculated points.

summary of the intensity changes of NFAT-LxVP is given in the bar graph of Figure 4D. Detailed inspection of Figure 4D suggests that the segment D384 to Q391 from the NFAT-LxVP peptide is tightly bound when adding CnAB, but it is also displaced again when adding GB1-PVIVIT. In contrast, the segment Y394 to L399 clearly binds CnAB but is not displaced by GB1-PVIVIT.

Interestingly, the latter segment contains the conserved WxK sequence, which thus seems to be important for the NFAT-LxVP peptide binding and responsible for the fact that the PVIVIT, or more generally the PxIxIT, peptides cannot fully displace the NFAT-LxVP peptide. Based on the K_D listed in Table 1, the addition of 75 μM CnAB to the sample of 62 μM NFAT-LxVP causes 90% of the peptide to be bound to CnAB. This agrees with the peak intensity changes for key residues L387-V389. The addition of four molar excess of the PVIVIT peptide used for this experiment should have resulted in complete displacement. Yet, some of the NFAT-LxVP residues remain bound. These observations suggest that both NFAT segments, the NFAT-LxVP and the PVIVIT, only partially compete for the same binding site and that the PVIVIT does not fully displace the NFAT-LxVP peptide. In addition, spectra of CnAB-bound ^{15}N-labeled NFAT-LxVP with and without unlabeled PVIVIT peptide are not identical. Thus, both peptides must bind simultaneously on the surface of CnAB. In order to test whether the same effects occur if only using CnA, we performed similar experiments with only CnA and obtained equivalent results as shown in Figure S2.

In a complementary experiment, we checked whether the peptide containing the LxVP motif can displace PRIEIT. We added nonlabeled CnAB to a sample of ^{15}N-labeled NFAT-PRIEIT peptide. Similar to the previous experiment, the competitor LxVP peptide was expressed with a GB1-tag, which was also used alone as negative control. Figure 5A shows the 2D HSQC spectrum of the free ^{15}N- NFAT-PRIEIT peptide (top panel). Addition of CnAB causes a subset of peaks to shift or disappear (middle panel). The cumulative loss of peak intensity indicates the complex formation of the PRIEIT peptide with CnAB. We then added the nonlabeled NFAT-LxVP peptide to examine whether it also partially competes out the PRIEIT (lower left panel). Unlike the previous experiment depicted in Figure 4, where the tighter binder GB1-PVIVIT was used, the two peptides examined here now have endogenous sequences and are with comparable affinities toward Cn (Table 1). Yet, when competing with a 4-fold excess of GB1-LxVP on exactly the same binding epitope, a full displacement of ^{15}N-NFAT-PRIEIT should occur according to the law of mass action. However, only a subset of the attenuated peaks reappears upon addition of the GB1-LxVP peptide. This confirms partial, but not full, competition between the NFAT-LxVP and NFAT-PRIEIT peptides. Two representative peaks are labeled

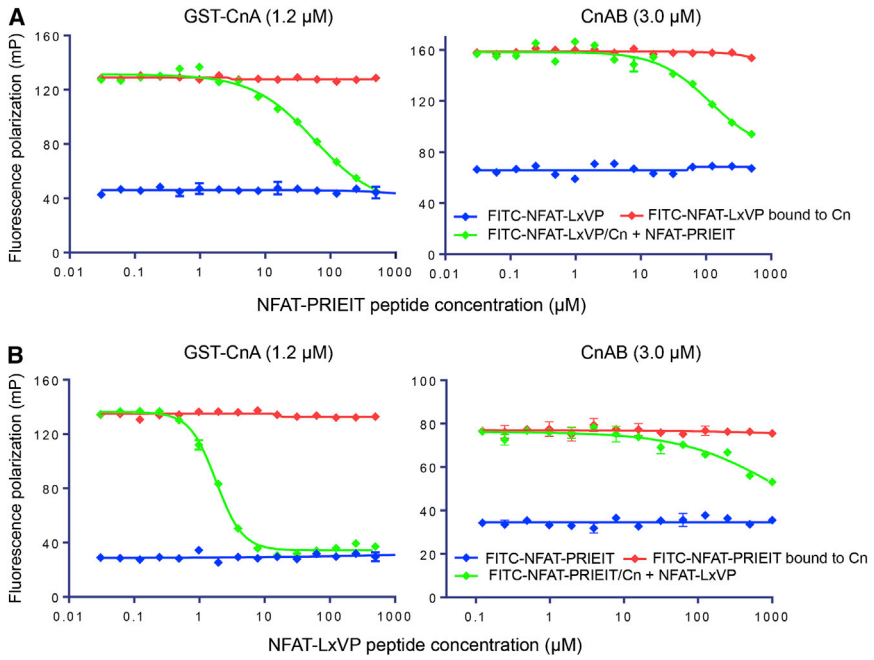

Figure 6. Monitoring the Displacement of NFAT-PRIEIT and NFAT-LxVP Peptides Using an FP Assay

(A) Displacement of the FITC-labeled NFAT-LxVP by the NFAT-PRIEIT peptide. Increasing concentrations of the NFAT-PRIEIT peptide were titrated into a mixture of 30 nM FITC-NFAT-LxVP peptide and 1.2 μM GST-CnA (left) and 3.0 μM CnAB (right).

(B) Displacement of the FITC-labeled PRIEIT by the LxVP peptide. Increasing concentrations of the LxVP peptide were titrated into a mixture of 30 nM FITC-PRIEIT peptide with 1.2 μM GST-CnA (left) and 3.0 μM CnAB (right). Note that the NFAT-derived PxIxIT and LxVP peptides will always be presented at equimolar concentrations as part of the same NFAT molecule. The experiment shown here documents that the two NFAT segments target the same epitope on CnA but do not displace each other as part of full-length NFAT.

in the spectra. The reappearance of residue E19 located in the PRIEIT motif suggests that its displacement from the binding epitope on Cn occurred following the addition of the NFAT-LxVP peptide. Thus, the data provide additional support that the PRIEIT and LxVP peptides bind to an overlapping region on Cn. The histogram in Figure 5B details the relative intensities of all NFAT-PRIEIT residues in each mode: free (black bars), bound to Cn (red bars) after the addition of GB1-LxVP (blue bars), and after the addition of GB1 as a negative control (green bars). It can be seen that the residues in the core of the binding motif exhibit the most pronounced intensity decrease upon CnAB binding as well as intensity recovery after LxVP addition. However, the observation that some residues do not fully recover after LxVP addition indicates simultaneous binding.

FP Experiments Confirm Competitive Binding of the PxIxIT and LxVP Peptides to CnA and CnAB

To further validate the competitive binding of the two NFAT derived peptides on both CnA and CnAB, we used a FP displacement assay. In Figure 6A, we labeled the NFAT-LxVP peptide with a fluorescein isothiocyanate (FITC) tag at its C terminus and incubated a 30 nM solution of the peptide with 1.2 μM of GST-CnA (left panel) or 3.0 μM heterodimer CnAB (right panel). To displace the FITC-labeled NFAT-LxVP peptide, we added increasing amounts of unlabeled NFAT-PRIEIT peptide. In each panel, the red and blue lines represent the constant amount of NFAT-LxVP peptide with and without the corresponding protein and without NFAT-PRIEIT. The green line represents the wells wherein increasing amounts of NFAT-PRIEIT peptide were added. It can be seen that the FITC-labeled 30 nM NFAT-LxVP peptide can be fully displaced at very high excess (~1,000-fold) of the NFAT-PRIEIT peptide in the mid to high micromolar range. Figure 6B exhibits the results of a complementary experiment wherein 30 nM FITC-PRIEIT peptide is incubated with 1.2 μM GST-CnA (left panel) or 3.0 μM of CnAB (right panel). Increasing concentrations of NFAT-LxVP peptide displaces the NFAT-PRIEIT peptide from both proteins. These data support the notion that both peptides bind to adjacent or overlapping epitopes on CnA. Note that higher concentrations of CnAB (3.0 μM) were used compared to GST-CnA (1.2 μM), whereas the concentration of the FITC-labeled peptide was the same. Thus, more titrant peptide is needed to displace the bound peptide, which shifts the FP displacement curves for CnAB to the right compared to those for GST-CnA. The fact that a large excess of one peptide is required to displace the other directly indicates that the overlap in the epitopes contributes only a modest amount to the overall affinity.

The high excess of NFAT-PRIEIT or NFAT-LxVP peptide over the other FITC-labeled peptide used here is different from the NMR competition experiment (Figure 5). In the NMR experiment, we used approximately equimolar amounts of both peptides at high micromolar concentrations. In vivo, the PRIEIT and LxVP segments will always be present at equimolar concentrations, because they are on the same NFAT molecule. Thus, the NMR competition experiments that showed simultaneous binding to the overlapping epitopes approximate this situation better. This is confirmed by the results of Figure 6. At the lowest titrant concentrations, we have equimolar concentrations, and the peptides do not displace each other, which is consistent with the equimolar NMR competition experiments described above. The fact that the separate peptides containing either the LxVP or the PxIxIT peptides can displace the other peptide at high excess supports the finding that the two NFAT peptides compete for the same binding site. The observation that displacement occurs at high excess of one peptide over the other indicates that the PxIxIT or LxVP peptides alone adapt bound structures that are incompatible with the other peptide binding. Only at approximately equal peptide concentrations a trimeric complex is formed where both peptides bind to CnA and interact with each other.

DISCUSSION

NFAT-specific inhibition of Cn in T cells has been an objective for obtaining safe immune-suppressing agents. Inhibitors broadly blocking the phosphatase activity of calcineurin, such as cyclosporin A or FK506, in complex with their cytoplasmic receptors cyclophilin and FKBP12, respectively, have been tremendously successful and are now routinely used to prevent rejection in organ transplants. However, the complete inhibition of Cn's enzymatic activity also affects all other functions of Cn outside the immune system and has severe side effects in the long-term treatment of transplant patients. Thus, there is a need for specific inhibitors for Cn's activity against NFAT only and not blocking its function in other contexts outside the immune system (Mullard, 2012). Indeed, initial inhibitors have been found already that prevent NFAT binding to Cn, its dephosphorylation, nuclear translocation, and upregulation of cytokines but do not inhibit its general phosphatase activity against other targets (Roehrl et al., 2004a, 2004c). Given the importance of this binding event, it is imperative to achieve a better structural understanding of the calcineurin-NFAT interaction, which would facilitate the search for novel NFAT-specific Cn inhibitors.

The discovery of two distinct Cn binding motifs, PxIxIT and LxVP, seemed to make it unlikely that the homology domain of NFAT could be displaced from Cn with a single molecule. This is in contrast to a previous study in which single compounds could inhibit NFAT dephosphorylation and nuclear translocation (Roehrl et al., 2004a, 2004c). Thus, a more detailed investigation of the interaction sites of the two binding peptides was desirable.

In this study, we embarked on defining the binding site of an NFAT-derived peptide containing the LxVP motif of NFATc1 on Cn. Using NMR spectroscopy, we discovered that the peptide containing the conserved NFAT-LxVP motif binds to the same CnA surface region as the high-affinity PVIVIT peptide. This finding was unexpected and is inconsistent with recent suggestions based on mutagenesis and modeling that locate the LxVP binding at the CnA/B interface (Rodríguez et al., 2009). Our findings are also contrary to the claim that the binding site of an LxVK sequence of the viral A238L protein represents NFAT's LxVP binding (Grigoriu et al., 2013). Besides the P/K difference, the viral protein also lacks the flanking sequences native to NFATs, including the WxK motif (Figure 1) that anchors the peptide onto CnA. Indeed, it has previously been shown that W/A mutation in the WxK motif impaired the inhibition activity of the mutated LxVP peptide (Rodríguez et al., 2009). Moreover, the binding affinity of the NFAT-LxVP peptide to Cn is similar to both the heterodimer CnAB and CnA alone (Table 1). This binding affinity also resembles that of the peptide containing the PxIxIT motif, which is known to bind explicitly to CnA. The similarity of the binding affinities indicates that the LxVP binding event manifests equal importance as the PxIxIT interaction. This is consistent with previous reports that peptides containing the LxVP sequence of NFATc1 (1) disrupt the NFAT/Cn interaction, (2) displace the PxIxIT peptide of NFATc2 from Cn, (3) prevent NFAT dephosphorylation, and (4) inhibit NFAT nuclear translocation (Martínez-Martínez et al., 2006).

The data presented here reveal that both peptides bind to epitopes on CnA that overlap but are not identical. The peptides containing the LxVP and PxIxIT motifs bind simultaneously when presented at equimolar concentrations as shown in Figures 4, 5, and 6. Equimolar concentrations resemble the binding event of the full-length NFAT, where both binding motifs are on the same polypeptide chain. Simultaneous binding at equimolar concentrations is also consistent with the FP displacement experiments of Figure 6, which show that the peptides cannot displace each other at the starting concentrations of the titration. For example, 30 nM FITC-NFAT-LxVP peptide could not be displaced from 1.2 μM CnA up to 10 μM PRIEIT concentration, and similar effects are observed in complementary titrations (Figure 6).

The fact that one peptide can displace the other at high excess, while binding to a common, but not entirely identical, epitope suggests the following model, which is visualized with the cartoon of Figure 7A. One peptide alone adopts a bound conformation that does not allow the other peptide to bind without changing its conformation (I and III). Thus, high excess of one peptide displaces the other. When both peptides are present at equal concentrations, they adopt a different trimeric conformation and do not dislocate each other (II). If one peptide is in excess, the equilibrium shifts to the conformation that is incompatible with the binding of the other peptide (transition from II to I or III). The three states are visible in the NMR experiment: the free NFAT-LxVP and NFAT-PxIxIT peptides are in Figures 4A and 5A; the dimeric complexes are in Figures 4B and 5B; and the trimeric complexes are at the left-hand side of Figures 4C and 5C with either ^{15}N-labeled LxVP or PxIxIT peptides. In the trimeric complexes, unlike the bound conformation with excess of each peptide, only parts of the peptides are tightly bound to the Cn surface, which is clearly seen from the uneven recovery of peptide signal intensities from dimeric to trimeric complex transition. It should be noted that the trimeric condition resembles the binding event of full-length NFAT with both motifs on the same polypeptide chain, where concentrations of both motifs are equal (IV).

It's unlikely, yet possible, that the isolated NFAT-LxVP peptide we used here may have different biophysical characteristics and hence bind differently than do the intact NHR. The PxIxIT and the LxVP segments might bind sequentially, so steric constraints could direct the LxVP to another site once the PxIxIT segment is already bound. To resolve this, cocomplex structures of Cn with the full-length NHR or even entire NFAT would be needed.

The NMR-derived location of the LxVP binding site is depicted in a surface representation of the CnAB heterodimer in Figure 7B. Relevant to this study, a previous report indicated that an LxVP-derived peptide inhibited dephosphorylation of the 19-residue phosphopeptide substrate for Cn (the phosphopeptide RII, D**LPVP**IPGRFDRRVpSVAAE), whereas the NFAT-PxIxIT peptide did not show such an inhibitory effect (Martínez-Martínez et al., 2006). This observation was used to support the notion that the LxVP and PxIxIT motifs bind at different sites, and based on docking studies, a putative LxVP binding epitope was predicted to reside at the CnA/B interface, overlapping with the immunosuppressant binding site (Rodríguez et al., 2009) (Figure 7B). However, the binding mode presented here can fully explain that earlier observation. The LxVP peptide directly competes with binding of the RII peptide, which contains an LxVP motif. This is not the case for the PxIxIT peptide, which can bind simultaneously.

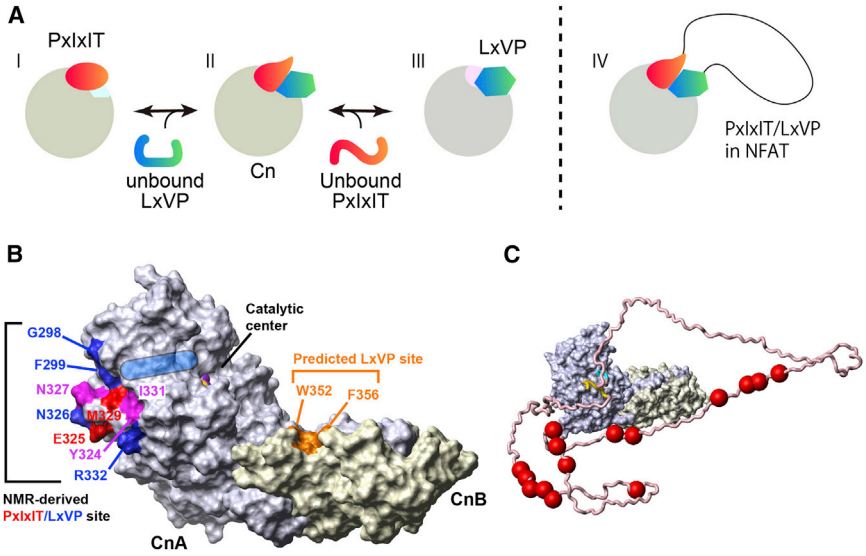

Figure 7. LxVP and PxIxIT Peptides Bind to an Overlapping Epitope on the CnAB Heterodimer

(A) Model for the conformational changes upon Cn interaction with different concentrations of LxVP- and PxIxIT-containing NFAT peptides. As suggested by the experimental data, LxVP (I) or PxIxIT (III) peptides alone form bound conformations incompatible with binding the other peptide. Equimolar concentration of the binding peptides leads to a trimeric bound structure of different conformation (II). The trimetric condition resembles the binding event of full-length NFAT, where both motifs are on the same polypeptide chain (IV).

(B) Location of the NMR-derived LxVP binding site on the surface representation of CnAB (Protein Data Bank ID code 1AUI). The residues of the NMR-derived LxVP and PxIxIT binding sites are colored blue and red, respectively, with the overlapping site colored in magenta. The groove connecting the LxVP binding site to Cn's catalytic center is shadowed in blue. The site in the CnA/B interface suggested in a previous study (Rodríguez et al., 2009) is marked in orange.

(C) Model of NFAT regulatory domain in complex with CnAB depicting simultaneous PxIxIT and LxVP binding to an overlapping epitope. The lowest energy model out of ten independent calculations using CYANA is shown (Herrmann et al., 2002). Phosphorylation sites are depicted with red spheres. The CnAB structures are shown in the same color as in (B).

In another experiment, it was shown that mutating CnA residues 330–332 from NIR to AAA did alter calcineurin activity toward the RII peptide as well (Li et al., 2004). This is now understandable because the Cn residues 330–332 are part of the PxIxIT binding site and therefore also part of our NMR-derived LxVP site. The fact that the RII peptide has an LxVP sequence suggests that the triple mutation disrupts the LxVP interaction at the overlapping epitope. The LxVP site within the RII peptide, which lacks the neighboring WxK motif, could have a different binding mode. But, in that case, the effects of the triple mutation would be difficult to explain.

Our experiments reported here do not support the LxVP peptide binding to a site between CnA and CnB subunits. The identification of the partially overlapping, but nonidentical, binding sites for the two NFAT segments is compatible with the different effects on dephosphorylation activity toward substrates. It should also be noted that inhibition of Cn's activity by the LxVP sequence does not diminish the importance of this site as a target for inhibiting NFAT dephosphorylation. Indeed, it was shown more than a decade ago that both binding motifs, PxIxIT and LxVP, need to be deleted to completely block NFAT dephosphorylation by Cn, supporting the essential role each of the sites plays in this interaction (Liu et al., 1999). Furthermore, our experimental data place the LxVP site at a distance of ~20 Å from calcineurin's active center, which is closer than the ~30 Å for the site predicted by the recent docking studies (Rodríguez et al., 2009). Considering the additional eight residues at the C terminus of the LxVP peptide used in the recent docking study, along with the physical proximity to the catalytic center of the site we found experimentally, an explanation is provided of how the LxVP peptide might be able to reach a site near Cn's active site and prevent access of the substrate peptide. Indeed, in the representation of Figure 7B, a groove can be seen connecting the LxVP site to Cn's catalytic center capable of accommodating the segment C-terminal to the LxVP motif in the peptide.

The observation that the two NFAT segments bind Cn simultaneously and do not displace each other at equimolar concentrations can readily explain earlier observations that addition of a PxIxIT-containing peptide cannot fully prevent the nuclear translocation process (Liu et al., 1999; Park et al., 2000). NFAT's regulatory domain can remain bound to the phosphatase by its LxVP motif. Our findings show that the LxVP-derived peptide binds to a site overlapped with the PxIxIT epitope, which resolves previous observations and establishes a distinct single Cn epitope as the key target for inhibiting the Cn/NFAT interaction.

The joint binding of the PxIxIT and LxVP motifs causes the regulatory domain to form a loop that contains all phosphorylation sites (Figure 7C). This loop formation can constrain the degrees of freedom of the bound NFAT regulatory domain and could induce formation of a localized structural architecture around the nuclear localization sequence and relate to the mechanism controlling translocation. In addition, loop formation of NFAT's regulatory domain has the advantage of shortening the distance of the phosphorylated residues to the active site and is expected to facilitate the dephosphorylation reaction on multiple sites (Figure 7B). Although the loop formation would also be expected if the LxVP and PxIxIT sites bind distinct regions on Cn, presence of the groove connecting the NMR-derived PxIxIT/LxVP binding site to Cn's catalytic center reveals an advantage of loop formation by the partially overlapping epitopes (Figure 7B).

Translocation of NFAT to the nucleus is a decisive event for T cell activation. It is triggered by calcium-induced activation of Cn and subsequent dephosphorylation of NFAT's regulatory domain. Elucidating the dynamic interplay of NFAT's Cn-binding segments provides crucial insight regarding the dephosphorylation process

and paves the way for understanding the nuclear translocation mechanism and T cell activation. In addition, our study opens an avenue for finding selective immunosuppressant drugs by relying on the structural aspects of Cn-NFAT interactions. Indeed, we are actively pursuing these questions via biophysical approaches in subsequent studies.

EXPERIMENTAL PROCEDURES

Expression and Purification of CnA

The catalytic domain of human calcineurin A (CnA), which includes residues 2–347 with the substitutions of Y341S, L343A, and M347D (Aramburu et al., 1998), was produced as a cleavable GB1 fusion protein containing a TEV cleavage recognition site in the *Escherichia coli* strain BL21 (DE3). Cleavage of the fusion protein with TEV protease produces CnA (2–347) with an additional Gly residue at its N terminus. CnA obtained is enzymatically active as described earlier (Roehrl et al., 2004a). Expression of ^{2}H,^{15}N-labeled CnA was obtained by growing *E. coli* in modified M9 Celtone medium, which consists of 1 kg/l 99.8% D2O, 6 g/l Na_2HPO_4, 3 g/l KH_2PO_4, 0.5 g/l NaCl, 40 mg/l carbenicillin, 1 g/l $^{15}NH_4Cl$ (99.9% enriched), 2 g/l $^{2}H_6$-$^{13}C_6$-glucose (97% enriched), 2 mM $MgSO_4$, 0.1 mM $CaCl_2$, 10 mg/l $ZnSO_4$, 10 mg/l $FeCl_3$, and 0.5g/l Celtone-based powder ^{2}H (>97% enriched), ^{13}C (>97% enriched), and ^{15}N (>98% enriched).

All expression experiments of labeled CnA were performed at 37°C. After reaching an optical density (OD; 600 nm) of 0.8, protein expression was induced by the addition of 1 mM isopropyl β-D-1-thiogalactopyranoside) (IPTG). The cells were harvested 36 hr after induction. The harvested cells were resuspended in 40 ml of 50 mM Tris-HCl (pH 8.0), 300 mM NaCl and 30 mM imidazole, 5 mM β-mercaptoethanol (β-ME), and 0.5% glycerol. The suspended cells were then disrupted by sonication, and the insoluble fraction was removed by centrifugation for 20 min at 15,000 *g*. The supernatant was applied to a 5 ml column of Nickel beads. After washing the resin with 40 ml of 50 mM Tris-HCl (pH 8.0), 300 mM NaCl, 30 mM imidazole, 5 mM β-ME, and 5% glycerol, the protein was eluted with PBS containing 5 mM β-ME and 300 mM imidazole. The elution fraction was concentrated to 4 ml by using 10,000 MWC membrane ultrafiltration. TEV protease was added to the concentrated elution fraction, and the solution was dialyzed with 1 l of PBS with 10 mM imidazole. The digested solution was applied to the Ni-NTA agarose column (QIAGEN) again and the flowthrough-containing CnA was further purified over a Superedex75 column (GE healthcare). A typical final yield of CnA was 2 mg/l culture.

Expression and Purification of Human Heterodimer CnAB

The plasmid for expressing the heterodimer calcineurin was obtained from Addgene (ID 11787) and was expressed as a tandem expression system as was previously described (Li et al., 2007; Mondragon et al., 1997). The heterodimer CnAB protein complex was further purified using a Ni-NTA agarose column (QIAGEN). After the His-tag was cleaved by overnight digestion with thrombin at 4°C, the protein solution was again passed through a Ni-NTA column followed by a Superdex200 size-exclusion column (GE healthcare).

Expression of the NFAT-LxVP, NFAT-PRIEIT, and PVIVIT-Containing Peptides

The NFAT-LxVP peptide containing the sequence 384-DQYLAVPQHPYQWAK-398 (NFATc1) was produced as a GB1 fusion protein in an *E. coli* strain, BL21 (DE3). The GB1 fusion protein has the PreScission protease recognition site between GB1 and NFAT-LxVP peptide, which added a GP dipeptide at its N terminus. For purification purposes, the construct was expressed with the LEHHHHHH tag at its C terminus. For expression of the uniformly $^{2}H^{15}N^{13}C$-labeled NFAT-LxVP peptide, *E. coli* harboring the GB1-NFAT-LxVP fusion vector was grown in M9 medium, which consists of 1 kg/l 99.8% D_2O, 6 g/l Na_2HPO_4, 3 g/l KH_2PO_4, 0.5 g/l NaCl, 50 mg/l Ampicilin, 1 g/l $^{15}NH_4Cl$ (99.9% enriched), 2 g/l $^{2}H_6$, $^{13}C_6$-glucose (97% enriched), 2 mM $MgSO_4$, and 0.1 mM $CaCl_2$. The cells were incubated at 37°C, and after reaching an OD (600 nm) of 0.7, protein expression was induced by the addition of 1 mM IPTG overnight in 25°C. The cells were harvested and resuspended in 40 ml of buffer A (50 mM Tris-HCl [pH 8.0], 300 mM NaCl, and 20 mM imidazole) with 0.2 mg/ml phenylmethanesulfonylfluoride (PMSF) at 4°C. The suspended cells were disrupted by sonication, and the insoluble fraction was removed by centrifugation at 15,000 *g* for 20 min. The supernatant was applied to a 5 ml column of Ni-NTA agarose. After washing the resin with 40 ml of buffer A, the GB1-NFAT-LxVP peptide was eluted with 40 ml of buffer consisting of 50 mM Tris-HCl (pH 7.5), 300 mM NaCl, and 300 mM imidazole. The elution fraction was concentrated to 2 ml by 3000 MWC-membrane ultrafiltration. PreScission protease and 1 mM DTT were added to the concentrated elution fraction. The digested solution was diluted with buffer A to reduce imidazole concentration to less than 30 mM and passed through Ni-NTA column. The peptide was eluted with PBS buffer at pH 3.4.

The NFAT-PRIEIT peptide contains the following $NFAT_{C2}$ sequence, which was produced as a GB1 fusion protein in an *E. coli* strain, BL21(DE3): WAAKPAGASGLSPRIEITPSHELIQAVGPLRM. The GB1 fusion protein has the TEV recognition site between GB1 and NFAT-PRIEIT peptide. For purification purposes, the construct was expressed with the LEHHHHHH tag at its N terminus. For the expression of uniformly $^{2}H^{15}N^{13}C$-labeled NFAT-PRIEIT peptide, *E. coli* harboring the correct plasmid was grown in M9 medium, which consists of 1 kg/l 99.8% D_2O, 6 g/L Na_2HPO_4, 3 g/l KH_2PO_4, 0.5 g/l NaCl, 50 mg/l Ampicilin, 1 g/l $^{15}NH_4Cl$ (99.9% enriched), 2 g/l $^{2}H_6$,$^{13}C_6$-glucose (97% enriched), 2 mM $MgSO_4$, and 0.1 mM $CaCl_2$. The cells were incubated at 37°C, and after reaching an OD (600 nm) of 0.7, protein expression was induced by the addition of 1 mM IPTG overnight at 25°C. The cells were harvested and resuspended in 40 ml of buffer A (50 mM Tris-HCl [pH 8.0], 300 mM NaCl, and 20 mM imidazole) with 0.2 mg/ml PMSF at 4°C. The suspended cells were disrupted by sonication, and the insoluble fraction was removed by centrifugation at 15,000 *g* for 20 min. The supernatant was applied to a 5 ml column of Ni-NTA agarose. After washing the resin with 40 ml of buffer A, the GB1-PxIxIT peptide was eluted with 40 ml of buffer consisting of 50 mM Tris-HCl (pH 7.5), 300 mM NaCl, and 300 mM imidazole. The elution fraction was incubated with TEV in the presence of 1 mM DTT and 0.5 mM EDTA overnight to allow for cleavage. The digested solution was diluted with buffer A (without Imidazole) to reduce imidazole concentration to less than 30 mM and passes through the Ni-NTA column. The flowthrough containing the peptide was collected followed by Superdex75 size-exclusion column chromatography.

The peptide containing the 15-residue PVIVIT sequence and His tag (GPHPVIVITGPHEELEHHHHHH) was expressed with similar procedures as described previously (Takeuchi et al., 2007).

NMR Spectroscopy

All experiments were performed on either Bruker Avance 500, 600, 750, or 800 MHz spectrometers equipped with cryogenic probes. All spectra were collected using 30 mM sodium phosphate buffer (pH 6.8) containing 150 mM NaCl, 1 mM dithiothreitol (DTT; in the experiments containing MTSL no DTT was used), and 90% H_2O/10% D_2O at 298 K. Spectra were processed using nmrPipe (Delaglio et al., 1995) and analyzed with SPARKY (Goddard and Kneller, 2008). The partial backbone assignment of CnA and the backbone assignment of the LxVP and PxIxIT peptides were accomplished using standard TROSY triple-resonance experiments as described previously (Takeuchi et al., 2007).

Fluorescence Polarization Assay

Fluorescence measurements were made on samples arrayed in 384-well plates by using an EnVision Multilabel Reader to monitor the interaction between Cn and FITC-labeled peptides. All measurements were done in triplicate. Experimental polarization data from simple and competitive binding experiments were fitted using GraphPad Prism6, with error bars representing SD.

Spin Labeling of a Single Cysteine Residue

A five molar excess of the MTSL spin label [(1-oxyl-2,2,5,5-tetramethylpyrroline-3-methyl)-methanesulfonothioate] was incubated with a Q385C mutant of the GB1-NFAT-LxVP protein sample for 4 hr at room temperature. Excess spin label was removed by size-exclusion chromatography using Superdex75 column. Further purification was done in a similar way to the LxVP peptide to remove GB1 and purify the resulting LxVP peptide.

Reagents and Chemicals

All chemicals were purchased from Sigma unless otherwise noted. Celtone powder was purchased from Spectra Stable Isotopes. MTSL for spin labeling was purchased from Toronto Research Chemicals.

SUPPLEMENTAL INFORMATION

Supplemental Information includes four figures, and one table and can be found with this article online at http://dx.doi.org/10.1016/j.str.2014.05.006.

AUTHOR CONTRIBUTIONS

G.W. conceived the overall project; M.G., S.L., and K.T. designed the experiments, made the samples, and performed the experiments. M.G., S.L., R.E.L., and G.W. wrote and revised the manuscript.

ACKNOWLEDGMENTS

This work was supported by a grant from the NIH (AI37581). Purchase, maintenance, and operation of the instruments used here were supported by NIH grants (GM047467 and EB002026). M.G. is grateful for a Human Frontier in Science Foundation postdoctoral fellowship. We thank Dr. Ricard Rodriguez for fruitful discussions and Dr. Huiming Li for useful discussion about the expression of CnAB obtained from Addgene.

Received: November 4, 2013
Revised: April 22, 2014
Accepted: May 4, 2014
Published: June 19, 2014

REFERENCES

Aramburu, J., Garcia-Cózar, F., Raghavan, A., Okamura, H., Rao, A., and Hogan, P.G. (1998). Selective inhibition of NFAT activation by a peptide spanning the calcineurin targeting site of NFAT. Mol. Cell *1*, 627–637.

Aramburu, J., Yaffe, M.B., López-Rodríguez, C., Cantley, L.C., Hogan, P.G., and Rao, A. (1999). Affinity-driven peptide selection of an NFAT inhibitor more selective than cyclosporin A. Science *285*, 2129–2133.

Arron, J.R., Winslow, M.M., Polleri, A., Chang, C.P., Wu, H., Gao, X., Neilson, J.R., Chen, L., Heit, J.J., Kim, S.K., et al. (2006). NFAT dysregulation by increased dosage of DSCR1 and DYRK1A on chromosome 21. Nature *441*, 595–600.

Chen, L., Glover, J.N., Hogan, P.G., Rao, A., and Harrison, S.C. (1998). Structure of the DNA-binding domains from NFAT, Fos and Jun bound specifically to DNA. Nature *392*, 42–48.

Crabtree, G.R., and Olson, E.N. (2002). NFAT signaling: choreographing the social lives of cells. Cell *109* (*Suppl*), S67–S79.

Delaglio, F., Grzesiek, S., Vuister, G.W., Zhu, G., Pfeifer, J., and Bax, A. (1995). NMRPipe: a multidimensional spectral processing system based on UNIX pipes. J. Biomol. NMR *6*, 277–293.

Flanagan, W.M., Corthésy, B., Bram, R.J., and Crabtree, G.R. (1991). Nuclear association of a T-cell transcription factor blocked by FK-506 and cyclosporin A. Nature *352*, 803–807.

Goddard, T.D., and Kneller, D.G. (2008). SPARKY 3. (San Francisco: University of California, San Francisco).

Graef, I.A., Chen, F., and Crabtree, G.R. (2001). NFAT signaling in vertebrate development. Curr. Opin. Genet. Dev. *11*, 505–512.

Griffith, J.P., Kim, J.L., Kim, E.E., Sintchak, M.D., Thomson, J.A., Fitzgibbon, M.J., Fleming, M.A., Caron, P.R., Hsiao, K., and Navia, M.A. (1995). X-ray structure of calcineurin inhibited by the immunophilin-immunosuppressant FKBP12-FK506 complex. Cell *82*, 507–522.

Grigoriu, S., Bond, R., Cossio, P., Chen, J.A., Ly, N., Hummer, G., Page, R., Cyert, M.S., and Peti, W. (2013). The molecular mechanism of substrate engagement and immunosuppressant inhibition of calcineurin. PLoS Biol. *11*, e1001492.

Gwack, Y., Sharma, S., Nardone, J., Tanasa, B., Iuga, A., Srikanth, S., Okamura, H., Bolton, D., Feske, S., Hogan, P.G., and Rao, A. (2006). A genome-wide Drosophila RNAi screen identifies DYRK-family kinases as regulators of NFAT. Nature *441*, 646–650.

Herrmann, T., Güntert, P., and Wüthrich, K. (2002). Protein NMR structure determination with automated NOE assignment using the new software CANDID and the torsion angle dynamics algorithm DYANA. J. Mol. Biol. *319*, 209–227.

Hogan, P.G., Chen, L., Nardone, J., and Rao, A. (2003). Transcriptional regulation by calcium, calcineurin, and NFAT. Genes Dev. *17*, 2205–2232.

Huai, Q., Kim, H.Y., Liu, Y., Zhao, Y., Mondragon, A., Liu, J.O., and Ke, H. (2002). Crystal structure of calcineurin-cyclophilin-cyclosporin shows common but distinct recognition of immunophilin-drug complexes. Proc. Natl. Acad. Sci. USA *99*, 12037–12042.

Ishiguro, K., Ando, T., Maeda, O., Watanabe, O., and Goto, H. (2011). Cutting edge: tubulin α functions as an adaptor in NFAT-importin β interaction. J. Immunol. *186*, 2710–2713.

Jain, J., McCaffrey, P.G., Valge-Archer, V.E., and Rao, A. (1992). Nuclear factor of activated T cells contains Fos and Jun. Nature *356*, 801–804.

Jin, L., Sliz, P., Chen, L., Macián, F., Rao, A., Hogan, P.G., and Harrison, S.C. (2003). An asymmetric NFAT1 dimer on a pseudo-palindromic kappa B-like DNA site. Nat. Struct. Biol. *10*, 807–811.

Kang, S., Li, H., Rao, A., and Hogan, P.G. (2005). Inhibition of the calcineurin-NFAT interaction by small organic molecules reflects binding at an allosteric site. J. Biol. Chem. *280*, 37698–37706.

Kao, S.C., Wu, H., Xie, J., Chang, C.P., Ranish, J.A., Graef, I.A., and Crabtree, G.R. (2009). Calcineurin/NFAT signaling is required for neuregulin-regulated Schwann cell differentiation. Science *323*, 651–654.

Kiani, A., Rao, A., and Aramburu, J. (2000). Manipulating immune responses with immunosuppressive agents that target NFAT. Immunity *12*, 359–372.

Kissinger, C.R., Parge, H.E., Knighton, D.R., Lewis, C.T., Pelletier, L.A., Tempczyk, A., Kalish, V.J., Tucker, K.D., Showalter, R.E., Moomaw, E.W., et al. (1995). Crystal structures of human calcineurin and the human FKBP12-FK506-calcineurin complex. Nature *378*, 641–644.

Lee, M., and Park, J. (2006). Regulation of NFAT activation: a potential therapeutic target for immunosuppression. Mol. Cells *22*, 1–7.

Li, H., Rao, A., and Hogan, P.G. (2004). Structural delineation of the calcineurin-NFAT interaction and its parallels to PP1 targeting interactions. J. Mol. Biol. *342*, 1659–1674.

Li, H., Rao, A., and Hogan, P.G. (2011). Interaction of calcineurin with substrates and targeting proteins. Trends Cell Biol. *21*, 91–103.

Li, H., Zhang, L., Rao, A., Harrison, S.C., and Hogan, P.G. (2007). Structure of calcineurin in complex with PVIVIT peptide: portrait of a low-affinity signalling interaction. J. Mol. Biol. *369*, 1296–1306.

Liu, J., Masuda, E.S., Tsuruta, L., Arai, N., and Arai, K. (1999). Two independent calcineurin-binding regions in the N-terminal domain of murine NF-ATx1 recruit calcineurin to murine NF-ATx1. J. Immunol. *162*, 4755–4761.

Macian, F. (2005). NFAT proteins: key regulators of T-cell development and function. Nat. Rev. Immunol. *5*, 472–484.

Martínez-Martínez, S., Rodríguez, A., López-Maderuelo, M.D., Ortega-Pérez, I., Vázquez, J., and Redondo, J.M. (2006). Blockade of NFAT activation by the second calcineurin binding site. J. Biol. Chem. *281*, 6227–6235.

Mondragon, A., Griffith, E.C., Sun, L., Xiong, F., Armstrong, C., and Liu, J.O. (1997). Overexpression and purification of human calcineurin alpha from Escherichia coli and assessment of catalytic functions of residues surrounding the binuclear metal center. Biochemistry *36*, 4934–4942.

Mullard, A. (2012). Protein-protein interaction inhibitors get into the groove. Nat. Rev. Drug Discov. *11*, 173–175.

Okamura, H., Aramburu, J., García-Rodríguez, C., Viola, J.P., Raghavan, A., Tahiliani, M., Zhang, X., Qin, J., Hogan, P.G., and Rao, A. (2000). Concerted dephosphorylation of the transcription factor NFAT1 induces a conformational switch that regulates transcriptional activity. Mol. Cell *6*, 539–550.

Okamura, H., Garcia-Rodriguez, C., Martinson, H., Qin, J., Virshup, D.M., and Rao, A. (2004). A conserved docking motif for CK1 binding controls the nuclear localization of NFAT1. Mol. Cell. Biol. *24*, 4184–4195.

Park, S., Uesugi, M., and Verdine, G.L. (2000). A second calcineurin binding site on the NFAT regulatory domain. Proc. Natl. Acad. Sci. USA *97*, 7130–7135.

Rao, A., Luo, C., and Hogan, P.G. (1997). Transcription factors of the NFAT family: regulation and function. Annu. Rev. Immunol. *15*, 707–747.

Rodríguez, A., Roy, J., Martínez-Martínez, S., López-Maderuelo, M.D., Niño-Moreno, P., Ortí, L., Pantoja-Uceda, D., Pineda-Lucena, A., Cyert, M.S., and Redondo, J.M. (2009). A conserved docking surface on calcineurin mediates interaction with substrates and immunosuppressants. Mol. Cell *33*, 616–626.

Roehrl, M.H., Wang, J.Y., and Wagner, G. (2004a). Discovery of small-molecule inhibitors of the NFAT—calcineurin interaction by competitive high-throughput fluorescence polarization screening. Biochemistry *43*, 16067–16075.

Roehrl, M.H., Wang, J.Y., and Wagner, G. (2004b). A general framework for development and data analysis of competitive high-throughput screens for small-molecule inhibitors of protein-protein interactions by fluorescence polarization. Biochemistry *43*, 16056–16066.

Roehrl, M.H., Kang, S., Aramburu, J., Wagner, G., Rao, A., and Hogan, P.G. (2004c). Selective inhibition of calcineurin-NFAT signaling by blocking protein-protein interaction with small organic molecules. Proc. Natl. Acad. Sci. USA *101*, 7554–7559.

Serfling, E., Berberich-Siebelt, F., Chuvpilo, S., Jankevics, E., Klein-Hessling, S., Twardzik, T., and Avots, A. (2000). The role of NF-AT transcription factors in T cell activation and differentiation. Biochim. Biophys. Acta *1498*, 1–18.

Shibasaki, F., Price, E.R., Milan, D., and McKeon, F. (1996). Role of kinases and the phosphatase calcineurin in the nuclear shuttling of transcription factor NF-AT4. Nature *382*, 370–373.

Takeuchi, K., Roehrl, M.H., Sun, Z.Y., and Wagner, G. (2007). Structure of the calcineurin-NFAT complex: defining a T cell activation switch using solution NMR and crystal coordinates. Structure *15*, 587–597.

Wolfe, S.A., Zhou, P., Dötsch, V., Chen, L., You, A., Ho, S.N., Crabtree, G.R., Wagner, G., and Verdine, G.L. (1997). Unusual Rel-like architecture in the DNA-binding domain of the transcription factor NFATc. Nature *385*, 172–176.

Wu, H., Peisley, A., Graef, I.A., and Crabtree, G.R. (2007). NFAT signaling and the invention of vertebrates. Trends Cell Biol. *17*, 251–260.

Zhou, P., Sun, L.J., Dötsch, V., Wagner, G., and Verdine, G.L. (1998). Solution structure of the core NFATC1/DNA complex. Cell *92*, 687–696.

Zhou, C.L., Lu, R., Lin, G., and Yao, Z. (2011). The latest developments in synthetic peptides with immunoregulatory activities. Peptides *32*, 408–414.

Zhu, J., Shibasaki, F., Price, R., Guillemot, J.C., Yano, T., Dötsch, V., Wagner, G., Ferrara, P., and McKeon, F. (1998). Intramolecular masking of nuclear import signal on NF-AT4 by casein kinase I and MEKK1. Cell *93*, 851–861.